Hindawi
Journal of Combustion
Volume 2021, Article ID 7111040, 13 pages
https://doi.org/10.1155/2021/7111040

Research Article

Combustion Characteristics and NO Formation Characteristics Modeling in a Compression Ignition Engine Fuelled with Diesel Fuel and Biofuel

Jean Paul Gram Shou,[1] **Marcel Obounou**,[1] **Rita Enoh Tchame**,[1] **Mahamat Hassane Babikir**,[1] **and Timoléon Crépin Kofané**[2]

[1]*Laboratory of Energy and Electronics and Electrical Systems, Department of Physics, Faculty of Science, University of Yaoundé I, P.O.Box 812, Yaoundé, Cameroon*
[2]*Laboratory of Mechanics, Materials and Structures, Department of Physics, Faculty of Science, University of Yaoundé I, P.O.Box 812, Yaoundé, Cameroon*

Correspondence should be addressed to Jean Paul Gram Shou; jpgram1085s@yahoo.fr

Received 18 June 2021; Revised 15 October 2021; Accepted 23 October 2021; Published 18 November 2021

Academic Editor: Kalyan Annamalai

Compression ignition engine modeling draws great attention due to its high efficiency. However, it is still very difficult to model compression ignition engine due to its complex combustion phenomena. In this work, we perform a theoretical study of steam injection being applied into a single-cylinder four-strokes direct-injection and naturally aspirated compression ignition engine running with diesel and biodiesel fuels in order to improve the performance and reduce NO emissions by using a two-zone thermodynamic combustion model. The results obtained from biodiesel fuel are compared with the ones of diesel fuel in terms of performance, adiabatic flame temperatures, and NO emissions. The steam injection method could decrease NO emissions and improve the engine performances. The results showed that the NO formation characteristics considerably decreased and the performance significantly increased with the steam injection method. The relative errors for computed nitric oxide concentration values of biodiesel fuel and diesel fuel in comparison to the measured ones are 2.8% and 1.6%, respectively. The experimental and theoretical results observed show the highly satisfactory coincidences.

1. Introduction

Engine simulation has been extensively used to improve the engine performance. Experimental work which is aimed at fuel economy and low pollutant emission for compression ignition engine requires change in input parameters which is not cost-effective. Thus, simulating the performance of internal combustion engines using mathematical models and powerful computers reduces the cost and time of experimental tests. In these simulation models, the effect of various design structures like design of combustion chamber input parameters and operational changes can be estimated in a fast and cheap way provided that main mechanism are recognized and modeled perfectly to meet the experimental results.

Petroleum products are the main sources of energy for internal combustion engines. However, rising prices for petroleum products, uncertain supplies, and even growing demand due to increasing population, improving living conditions, and stricter emission standards have triggered intensive research for biofuels [1, 2]. The continuous demand of finding alternative fuels and reducing emissions has motivated the development of numerical models to provide predictive tools for designers. Engine simulation has therefore become an important part of the internal combustion engine design process to improve engine performance [3–10].

Zheng et al. [11] used a single-zone model with detailed kinetics in order to determine the general trends of autoignition characteristics, engine performance, and nitric

oxides emission as functions of major operating parameters for a natural gas-fuelled HCCI engine. In their study, the chemical kinetics employed is GRI-Mech 3.0, which includes 53 species and 325 elementary reactions, and it has been developed for gas phase natural reactions and includes hydrocarbon species up to C_3 and the problem with natural gas; it is hard to autoignite and therefore requires a higher compression ratio, some amount of intake heating, or some type of preignition. Huanhuan et al. [12] conducted a theoretical study on the effects of H_2O and CO_2 dilution in the oxidizer or fuel stream on counterflow methane diffusion flames, emphasizing NO formation kinetics. Their results showed that the impact of different radiation heat transfer models on NO emissions diminishes with increase in the dilution ratio. Dhana Raju et al. [13] examined the engine characteristics by focusing on the effect of various oxygenated additives such as diethyl ether, dimethyl ether, and dimethyl carbonate on 20% tamarind seed methyl ester biodiesel blend of different concentrations (6% and 12%) in volume basis. Their results showed that 12% diethyl ether added to 20% tamarind seed methyl ester shows considerable enhancement in brake thermal efficiency, which is 4.22% higher than of tamarind biodiesel blend. Dhana Raju et al. [14] examined the viability of tamarind biodiesel as an alternative fuel for diesel engine applications. They investigated the influence of nanoparticles as fuel-borne catalysts on 20% tamarind biodiesel blend and concluded that significant enhancement in brake thermal efficiency and considerable reduction in engine harmful exhaust emissions can be achieved.

The performance of compression ignition engines could be reduced and NO_x emissions could be increased with the addition of ethanol to diesel fuel [15–22]. Some techniques can be used such as EGR, water, and steam injection into combustion chamber to reduce these adverse effects of the ethanol mixtures on diesel engines [23–28]. Although, EGR is commonly used to minimize NO_x emissions, performance is dramatically decreased [23, 24]. Water injection into the engine combustion chamber with different methods is another NO_x reduction technique [25, 26]. One of the substantial handicaps of water injection techniques is that condensed water in the cylinder downgrades the quality of lubrication oil and raises the attrition rate of moving parts of the engine [28]. Recently, one of the developed techniques to reduce NO_x emissions and improve the engine performance is the steam injection method [28–31]. Gonca et al. [26, 27] conducted a theoretical study on the steam injected diesel engine and miller cycle diesel engine using a two-zone combustion model. The results of the study showed that steam injection could minimize NO_x emissions from diesel engines and improve effective efficiency and effective power. Parlak et al. [28] developed an electronically controlled steam injection method for a diesel engine. When this technique was implemented to diesel engine, NO_x emissions decreased up to 33%, effective power and torque increased up to 3%, and specific fuel consumption minimized up to 5% at full-load tests. Cesur et al. [29] and Kökkülünk et al. [30] applied the electronically controlled steam injection system into gasoline and diesel engines, and they obtained similar results to those of Parlak et al.'s study [28]. In these studies, the optimum steam ratio was determined as 20% of injected fuel by mass in terms of NO_x reduction and performance improvement. Therefore, the steam injection method could be implemented to a diesel engine fuelled with ethanol-diesel mixture so as to improve performance and reduce NO_x emissions.

Conventional fuels like diesel fuels, aviation fuels, and biodiesel fuels are composed of many different classes of hydrocarbons, and hence, it would be impossible to conduct meaningful experiments and simulation with such a vast number of chemicals contained in one mixture. In order to overcome this problem, surrogate fuels are used. These are well-defined mixtures of a small number of hydrocarbon compounds whose relative concentrations can be adjusted so that the physical and chemical properties of their combustion approximate those of a fuel that is difficult to study theoretically and experimentally.

Equilibrium mole fractions and adiabatic flame temperature are necessary for not only estimating thermodynamic properties of exhaust NO but also providing key data to obtain the nonequilibrium concentrations. The model used in this study is based on a recourse to identify convenient surrogate fuels, and it can simulate steam injection. In addition, it used computed thermodynamic properties of combustion products more accurately than the existing combustion, which are used in thermodynamic analysis of internal combustion engines. Methyl butyrate thermodynamic data were used as the surrogate for biodiesel fuel. In this study, the effects of steam injection into a diesel engine fuelled with diesel and biodiesel fuels have been studied in terms of performance and NO emissions using a two-zone thermodynamic model.

2. Materials and Methods

2.1. Specifications of the Diesel Engine. Tests were carried out on a four-stroke single-cylinder naturally aspirated direct-injection stationary compression ignition engine at constant speed. The specifications of the engine are given in Table 1.

The physical and chemical properties of the fuels are presented in Table 2.

The injected steam should not be regarded as an ideal gas since its specific heat strongly depends on pressure. In our case, the temperature of unburned mixture is found by assuming a thermal equilibrium among the reactants and the pressure inside the combustion chamber is taken as 30 atm. which is assumed equal to the pressure of injected steam. The temperature of injected steam at 30 atm. is 300°C corresponding to steam phase. The water should be heated by the engine coolant and exhaust gas in order to obtain the injected steam. The schematic diagram of the steam injection method is shown in Figure 1.

2.2. Theoretical Model

2.2.1. Heat Transfer Submodel. The heat transfer into the system is expressed in terms of heat loss from the burned and unburned gas, respectively.

Table 1: Specifications of the diesel engine.

Power output at 1500 rpm	4.5 kW
Engine cooling system	Air cooled
Intake system	Naturally aspirates
Bore and stroke (mm)	95.3/88.9
Displacement volume (cm^3)	630
Number of cylinders	1
Compression ratio	18 : 1

Table 2: Chemical and physical properties of test fuels.

Fuel properties	Diesel fuel	Biodiesel fuel
Density at 15°C ($kg\,m^{-3}$)	853.7	865.19
Kinematic viscosity at 40°C ($mm^2\,s^{-1}$)	2.8271	3.5
LHV ($kJ.kg^{-1}$)	42640	37000
Oxygen (wt.%)	0.00	11.27
Cetane number	42.6	54
Chemical formula	$C_{14.09}H_{24.78}$	$C_{18}H_{36}O_2$

$$\frac{dQ_h}{d\theta} = -\frac{\dot{Q}_l}{\omega} = -\frac{\dot{Q}_b + \dot{Q}_u}{\omega}, \tag{1}$$

$$\begin{aligned} \dot{Q}_b &= h_c A_b (T_b - T_W), \\ \dot{Q}_u &= h_c A_u (T_u - T_W), \end{aligned} \tag{2}$$

where h_c is the convectional heat transfer coefficient between the gas mixture and cylinder walls and A_b and A_u are the areas of burned and unburned gas in contact with the combustion chamber walls at temperature T_W. The convectional heat transfer coefficient is determined using Woschni correlation given by

$$\begin{aligned} h_c &= 3.26 b^{-0:2} p^{0.8} \left(\mathrm{xT}_b + (1-x)T_u\right)^{-0.55} w^{0.8}, \\ w &= C_1 V_p + C_2 \frac{V_d T_r}{p_r V_r} (p - p_{motored}), \end{aligned} \tag{3}$$

where b is the bore diameter of the cylinder, w is the mean gas velocity in the cylinder, and x is mass fraction burned. C_1 and C_2 are constants that depend on the stroke of the cycle. V_P is the mean piston speed, p_r, T_r, and V_r, are pressure, temperature, and cylinder volume at intake valve closing, and $p_{motored}$ is the pressure of the engine at the motored cycle.

The fraction of cylinder area contacted by burned gas is assumed to be proportional to the square root of the mass fraction burned to reflect the fact that burned gas occupies a larger volume fraction of the cylinder than the unburned gas due to the density difference between burned and unburned gas. The areas of burned and unburned gas are calculated using the following relations:

$$\begin{aligned} A_b &= \left(\frac{\pi b^2}{2} + \frac{4V}{b}\right)\sqrt{x}, \\ A_u &= \left(\frac{\pi b^2}{2} + \frac{4V}{b}\right)(1 - \sqrt{x}), \end{aligned} \tag{4}$$

2.2.2. Fuel Injection Submodel. The fuel injection rate $\dot{m}_{fi}$ is determined empirically from the fuel injection rate [32].

$$\frac{\dot{m}_{fi}}{m_{fi}} = \frac{\omega}{\theta_d \Gamma(n)} \left(\frac{\theta - \theta_s}{\theta_d}\right)^{n-1} \exp\left(-\frac{(\theta - \theta_s)}{\theta_d}\right), \tag{5}$$

where $\Gamma(n)$, θ_s, θ_d, and $\dot{m}_{fi}$ are the gamma function, the start angle of injection, the injection duration, and the total mass of fuel to be injected, respectively. The gamma function and the total injected fuel mass are expressed as [32]

$$\begin{aligned} \ln \Gamma(n) = &\left(n - \frac{1}{2}\right) \ln(n) - n + \frac{1}{2} \ln(2\pi) + \frac{1}{12n} - \frac{1}{360n^3} \\ &+ \frac{1}{1260n^5} - \frac{1}{1680n^7}, \end{aligned} \tag{6}$$

where n is an integer and its value could be taken for the diesel engine with open chamber as $1 \le n \le 2$ and for close chamber as $3 \le n \le 5$.

$$m_{fi} = \phi \mathrm{FA}_s (1 - \mathrm{RGF}) m_a. \tag{7}$$

2.2.3. Ignition Delay Submodel. The correlation proposed by Hardenberg and Hase [31] is used to calculate the ignition delay in crank angle degrees, and it is given by

$$\begin{aligned} \tau_{ig} = &\left(0.36 + 0.22 V_p\right) \\ &\times \exp\left[E_A\left(\frac{1}{\mathrm{RT}} - \frac{1}{17,190}\right) + \left(\frac{21.2}{p - 12.4}\right)^{0.63}\right]. \end{aligned} \tag{8}$$

The value of the apparent activation energy was determined using the following expression:

$$E_A = \frac{618{,}840}{\mathrm{CN} + 25}. \tag{9}$$

2.2.4. Mass Change in the Cylinder. The rates of change of burned fuel and air in the cylinder are determined as follows:

$$\begin{aligned} \frac{dm_f}{d\theta} &= \frac{1}{\omega}\left(\dot{m}_{fi} - \frac{\dot{m}_l \phi \mathrm{FA}_s}{1 + \phi \mathrm{FA}_s}\right), \\ \frac{dm_a}{d\theta} &= -\frac{\dot{m}_l}{\omega\left(1 + \phi \mathrm{FA}_s\right)}, \end{aligned} \tag{10}$$

where $\dot{m}_l$, ϕ, and FA_s are the gas leak rate, equivalence ratio, and stoichiometric fuel/air ratio by mass, respectively.

The burned gas leaking through the rings is expressed as

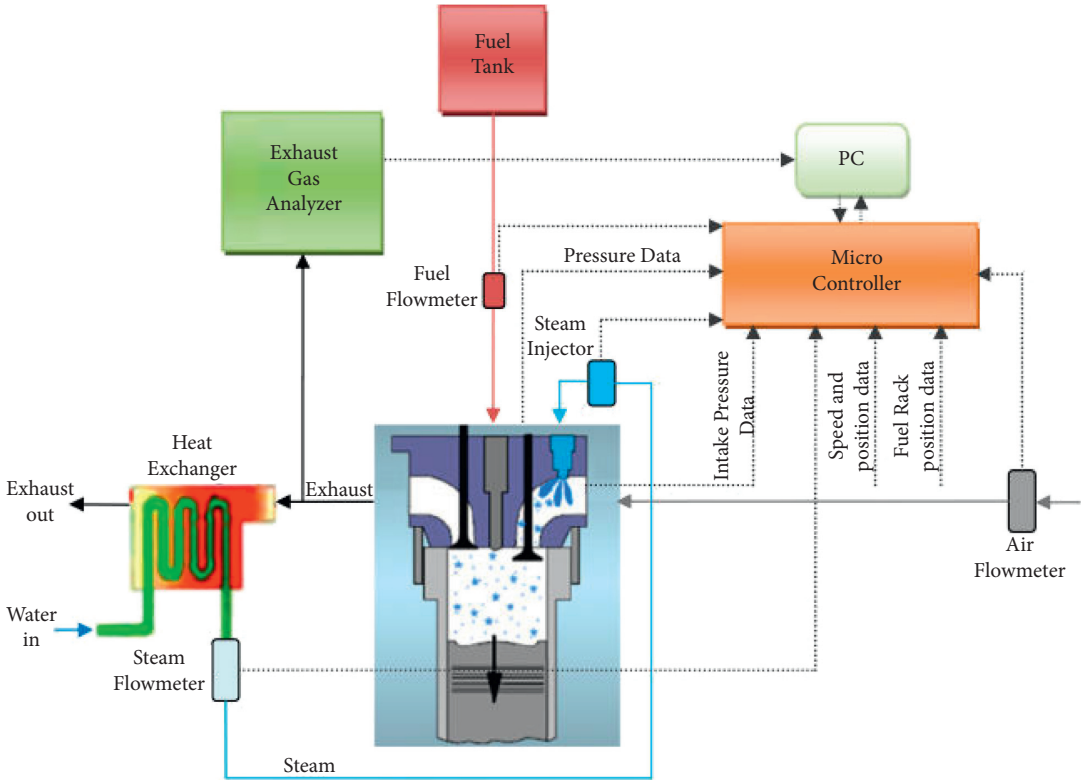

Figure 1: Schematic diagram of the steam injection method [32].

$$\frac{dm_l}{d\theta} = \frac{mC_b}{\omega}, \tag{11}$$

where C_b and ω are the blowby coefficient and angular velocity, respectively.

The total mass inside the cylinder at any time can be expressed as

$$m = m_{fi} + m_a. \tag{12}$$

2.2.5. Energy Equation. Combustion simulation of diesel engine fuelled by diesel and biodiesel is carried out by using a two-zone combustion model in order to calculate NO emissions, effective efficiency, and power. The burned and unburned zones are divided by the region border. In the combustion chamber, the equation of the energy conservation in differential form is given by

$$m\frac{du}{d\theta} + u\frac{dm}{d\theta} = -\frac{dQ_b}{d\theta} - \frac{dQ_u}{d\theta} - p\frac{dV}{d\theta} + \frac{dm_f}{d\theta}h_f - \frac{dm_l}{d\theta}h_l, \tag{13}$$

where m_l is the leak mass, m_f is the mass of injected fuel, and h_f and h_l are the enthalpies of injected fuel and leak mass per cycle, respectively.

The mass fraction burned x is defined using dual Wiebe function, and it is used to express the heat release from the combustion.

The differential equation used to calculate the pressure is given by

$$\frac{dp}{d\theta} = \frac{A + B + C}{D + E}. \tag{14}$$

The temperatures in the burned and unburned zones are calculated using the following differential equations:

$$\frac{dT_b}{d\theta} = \frac{-h_c\left(\pi b^2/2 + 4V/b\right)\left(T_b - T_W\right)}{m\omega c_{pb}\sqrt{x}} + \frac{v_b}{c_{pb}}\frac{\partial \ln v_b}{\partial \ln T_b}\left(\frac{A + B + C}{D + E}\right) + \frac{h_u - h_b}{xc_{pb}}\left[\frac{dx}{d\theta} - \left(x - x^2\right)\frac{C_b}{\omega}\right], \tag{15}$$

$$\frac{dT_u}{d\theta} = \frac{-h_c\left(\pi b^2/2 + 4V/b\right)\left(T_u - T_W\right)}{m\omega c_{pu}\left(1 + \sqrt{x}\right)} + \frac{v_u}{c_{pu}}\frac{\partial \ln v_u}{\partial \ln T_u}\left(\frac{A + B + C}{D + E}\right), \tag{16}$$

where

$$A=\frac{1}{m}\left(\frac{\mathrm{d}V}{\mathrm{d}\theta}+\frac{\mathrm{VC}_b}{\omega}\right),$$

$$B=\frac{h_c\left(\pi b^2/2+4V/b\right)}{m\omega}\left[\begin{array}{l}\dfrac{v_b}{c_{pb}}\dfrac{\partial \ln v_b}{\partial \ln \mathrm{T}_b}\sqrt{x}\,\dfrac{T_b-T_W}{T_b}\\[2ex] +\dfrac{v_u}{c_{pu}}\dfrac{\partial \ln v_u}{\partial \ln \mathrm{T}_u}(1-\sqrt{x})\dfrac{T_u-T_W}{T_u}\end{array}\right],$$

$$C=-\left(v_b-v_u\right)\frac{\mathrm{d}x}{\mathrm{d}\theta}-v_b\frac{\partial \ln v_b}{\partial \ln \mathrm{T}_b}\frac{h_u-h_b}{c_{pb}T_b}\left[\frac{\mathrm{d}x}{\mathrm{d}\theta}-\left(x-x^2\right)\frac{C_b}{\omega}\right],$$

$$D=x\left[\frac{{v_b}^2}{c_{pb}T_b}\left(\frac{\partial \ln v_b}{\partial \ln \mathrm{T}_b}\right)^2+\frac{v_b}{p}\frac{\partial \ln v_b}{\partial \ln \mathrm{p}}\right],$$

$$E=(1-x)\left[\frac{{v_u}^2}{c_{pu}T_u}\left(\frac{\partial \ln v_u}{\partial \ln \mathrm{T}_u}\right)^2+\frac{v_u}{p}\frac{\partial \ln v_u}{\partial \ln \mathrm{p}}\right],$$

$$\frac{\mathrm{d}W}{\mathrm{d}\theta}=p\frac{\mathrm{d}V}{\mathrm{d}\theta},$$

$$\frac{\mathrm{d}H_l}{\mathrm{d}\theta}=\frac{\mathrm{mC}_b}{\omega}\left(\left(1-x^2\right)h_u+x^2h_b\right),$$

$$\frac{\mathrm{dQ}_l}{\mathrm{d}\theta}=\frac{h_c\left(\pi b^2/2+4V/b\right)}{\omega}\left[\sqrt{x}\left(T_b-T_W\right)+(1-\sqrt{x})\left(T_u-T_W\right)\right]. \tag{17}$$

2.2.6. Zeldovich Mechanism. NO emissions are calculated using Zeldovich mechanism [33] which takes into account 10 combustion products provided by the chemical equilibrium model [34], and it is given as follows:

$$N_2+O\rightleftarrows \mathrm{NO}+N;\ k_{1f}=1.8\times10^8\exp\left(\frac{-38,370}{T}\right), \tag{18}$$

$$N+O_2\rightleftarrows \mathrm{NO}+O;\ k_{2f}=1.8\times10^4\mathrm{T}\exp\left(\frac{-4,680}{T}\right), \tag{19}$$

$$N+\mathrm{OH}\rightleftarrows \mathrm{NO}+H;\ k_{3f}=7.1\times10^7\exp\left(\frac{-450}{T}\right). \tag{20}$$

Three assumptions are applied to chemical reaction equations (18)–(20) to result in equation (21). The first assumption applied is that the nitrogen chemistry is decoupled from the combustion reactions, the second assumption applied is that O, H, and OH radicals are at their equilibrium concentration at equilibrium temperature, and finally, the third assumption is that nitrogen radical (N) is at pseudo-steady state; the free nitrogen atoms are consumed as rapidly as they are generated. The rate of NO formation can be determined by using the differential equation given as

$$\frac{\mathrm{d}\alpha}{\mathrm{d}t}=\frac{1}{[\mathrm{NO}]_e}\frac{2R_1\left(1-\alpha^2\right)}{1+K\alpha}, \tag{21}$$

where α stands for equilibrium concentration ratio, and it is given as

$$\alpha=\frac{[\mathrm{NO}]}{[\mathrm{NO}]_e}. \tag{22}$$

The other constants used in equation (21) are expressed as follows:

$$\begin{aligned}K&=\frac{R_1}{R_2+R_3},\\ R_1&=k_{1f}[\mathrm{N}_2]_e[\mathrm{O}]_e=k_{1r}[\mathrm{NO}]_e[\mathrm{N}]_e,\\ R_2&=k_{2f}[\mathrm{N}]_e[\mathrm{O}_2]_e=k_{2r}[\mathrm{NO}]_e[\mathrm{O}]_e,\\ R_3&=k_{3f}[\mathrm{N}]_e[\mathrm{OH}]_e=k_{3r}[\mathrm{NO}]_e[\mathrm{H}]_e.\end{aligned} \tag{23}$$

Equation (21) is integrated at each mass fraction burned x from the crank angle at which that element initially burns to a crank at which the reaction rates are negligible. At this crank angle, the diminished value of the NO mole fraction y_{NO_d} is achieved. The overall mole fraction of NO is given by

$$y_{\mathrm{NO}}=\int_0^1 y_{\mathrm{NO}_d}(x)\mathrm{d}x. \tag{24}$$

2.3. Engine Performance Parameters. The engine performance parameters are determined from the relations as follows. The composite Simpson's rule approximates the integral of IMEP by

$$\mathrm{IMEP}=\sum_{i=0}^{n}\frac{\left(V_{i+1}-V_i\right)\left(p_{2i}+4p_{2i+1}+p_{2i+2}\right)}{3V_d}. \tag{25}$$

The BMEP is defined as

$$\mathrm{BMEP}=\mathrm{IMEP}-\mathrm{FMEP}. \tag{26}$$

Here, FMEP is determined the following correlation [31]:

$$\mathrm{FMEP}=\frac{\tau-4}{14.5}+4.83\times10^{-4}N+0.103\left(\frac{V_P}{5.05}\right)^2. \tag{27}$$

where τ is the volumetric compression ratio.

Brake torque is defined as

$$\tau_e=\frac{\mathrm{BMEP}\times V_d}{4\pi}. \tag{28}$$

The BTE expresses the percentage of fuel energy converted to useful power output:

$$\eta_e=\frac{P_e}{\dot{m}_f\times\mathrm{LHV}_f}. \tag{29}$$

The BSFC represents the ratio of mass fuel injection to the combustion chamber per unit brake power output, and it is expressed as follows:

$$\mathrm{BSFC}=\frac{3600\times\dot{m}_f}{P_e}. \tag{30}$$

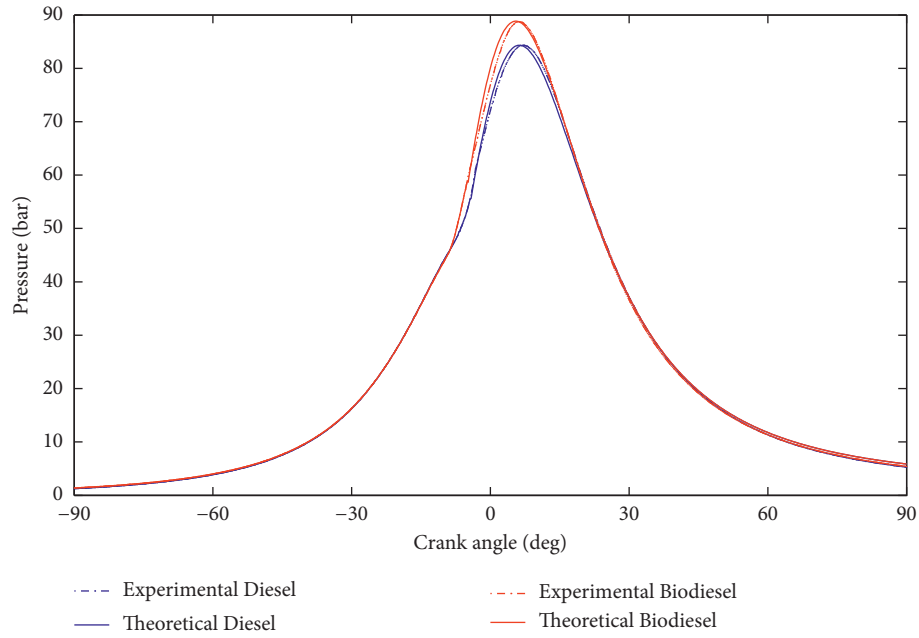

Figure 2: Comparison of experimental and theoretical pressures for biodiesel and diesel fuels.

3. Results and Discussion

3.1. Combustion Characteristics

3.1.1. In-Cylinder Pressure. The comparison of numerical and experimental pressures against the crank angle for biodiesel fuel with the ones for diesel fuel at full-load conditions is indicated in Figure 2. The peak pressure for the biodiesel fuel exceeds the one for diesel fuel due to the higher oxygen contents and CN of the biodiesel. The oxygen content, vaporization, and CN of fuels may influence the mass fraction burned. CN is one of the most important factors that influence the peak pressure. A higher CN normally corresponds to reducing the ignition delay period, reducing the premixing time, and moving the combustion phase earlier to the compression stroke as shown in Figures 3 and 4. In a compression ignition engine, the peak pressure in the combustion chamber depends on the burned fuel fraction during the premixed burning phase in the initial combustion stages and a longer ignition delay may lead to a higher maximum peak pressure in the combustion chamber.

3.1.2. Heat Release Rate. Figure 5 shows the heat leakage rate against the crank angle for biodiesel fuel compared to the one for diesel fuel at 100% of load. There are differences in heat leakage rate curves. The higher heat leakage rate of biodiesel fuel in the combustion stroke can be due to its higher equivalence ratio and its higher mass injected per cycle.

Figure 6 shows the heat transfer against the crank angle for biodiesel fuel compared to the one for diesel fuel at 100% of load. The picture shows that the value of heat transfer rate of biodiesel fuel is slightly higher than the one of diesel fuel despite its lower calorific value. This heat transfer rate of biodiesel fuel can be explained by the oxygen content and the earlier start of combustion. The oxygen content leads to complete combustion and vaporization and CN which are responsible for the earlier start of combustion. The heat transfer of biodiesel fuel in the combustion stroke can be also due to its higher equivalence ratio and its higher mass injected per cycle.

Figure 7 shows the work against the crank angle for biodiesel fuel compared to the one for diesel fuel at 100% of load. The work remains constant during the compression stroke and increases during combustion stroke due to the combustion. As a fluid element burns, its expansion compresses both unburned and burned gases. Because the volume per unit mass of the hot burned gas is larger than the one of the cooler unburned gas, the increase in the mass specific internal energy due to the compression work is higher for burned gas than for unburned gas. The slightly higher predicted value of cumulative work done by biodiesel fuel than the one by diesel fuel is due to increase in the heat release rate and peak pressure.

3.2. Performance Characteristics

3.2.1. Performance Parameters. At full-load condition (4.5 kW), the brake power values are found, by simulation, to be 4.43 kW and 4.52 kW for biodiesel fuel and diesel fuel, respectively. Biodiesel fuel has lower heating value than diesel fuel and hence produces slightly less power.

The lower calorific value and the higher kinematic viscosity are responsible for the poor atomization of biodiesel in the combustion chamber of the engine and tend to reduce BTE [29]. The diesel fuel has the highest BTE, which is probably because of its lower viscosity than the biodiesel fuel. Higher viscosities and densities of biodiesel affect fuel atomization; this results in biodiesel having a lower BTE than diesel fuel.

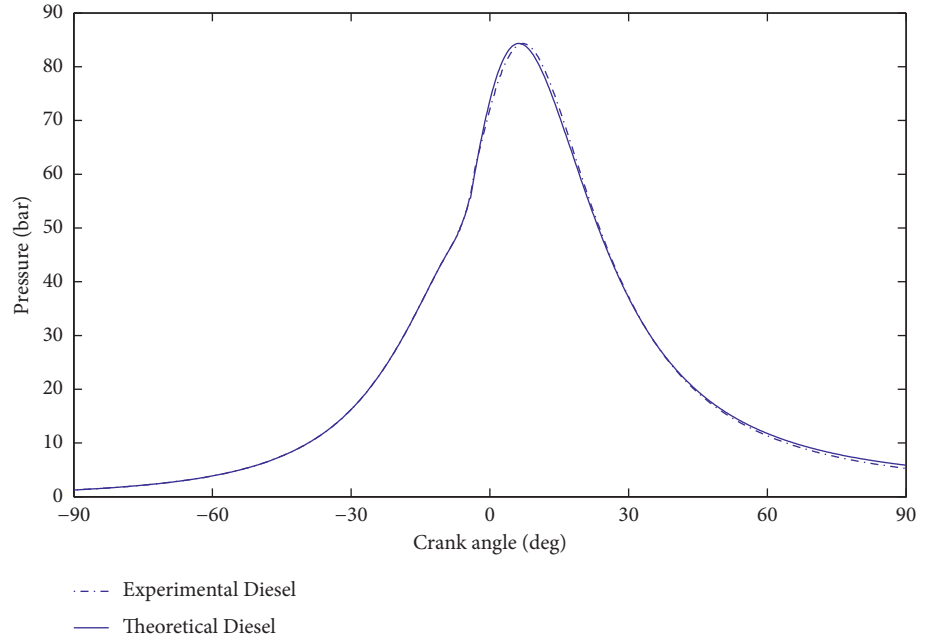

Figure 3: Comparison of experimental and theoretical pressures for diesel fuel.

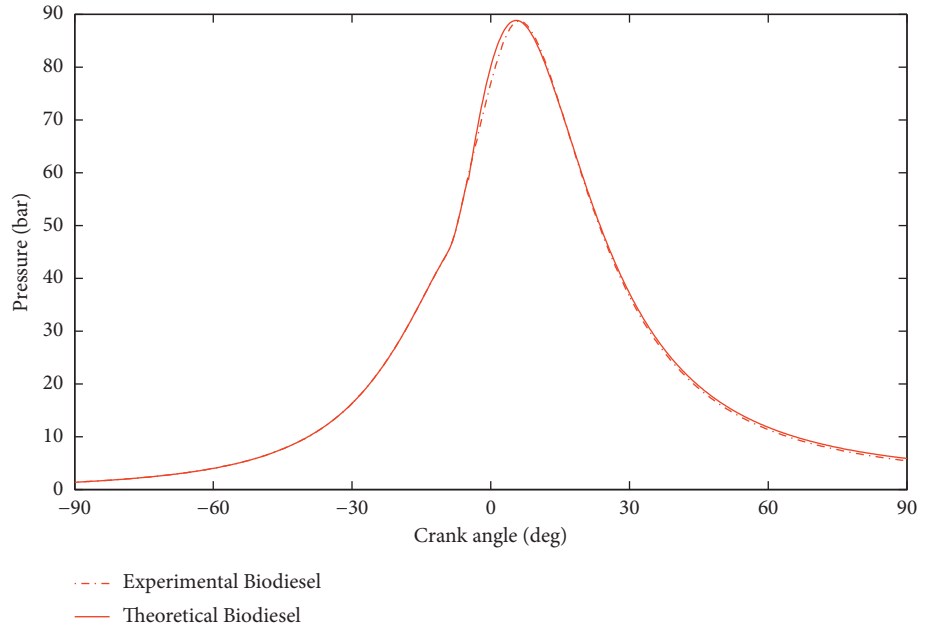

Figure 4: Comparison of experimental and theoretical pressures for biodiesel fuel.

The respective average decrease in brake torque and engine power values of the biodiesel fuel at 1500 rpm is 1.99% and 1.98% because of the higher viscosity, higher density, and lower heating (12.39%) as compared to pure diesel fuel. It was noticed that there was no significant difference in engine power between biodiesel fuel and diesel fuel. The recovery in brake torque and engine power for biodiesel fuel related to diesel fuel can be explained by the higher viscosity of biodiesel fuels which ameliorate fuel spray penetration and improve air-fuel mixing.

The BSFC for the biodiesel fuel and diesel fuel are 299.17 g/kWh and 240.15 g/kWh, respectively. It was seen that BSFC for the diesel fuel was less than the one for biodiesel fuel. The calorific value of biodiesel fuel is lower than the one of diesel fuel, and this fact explains the abovementioned results of BSFC.

3.2.2. Exhaust Gas Temperature. The comparison of theoretical in-cylinder temperatures at full-load conditions for the engine speed rate tested is given in Figure 8. The

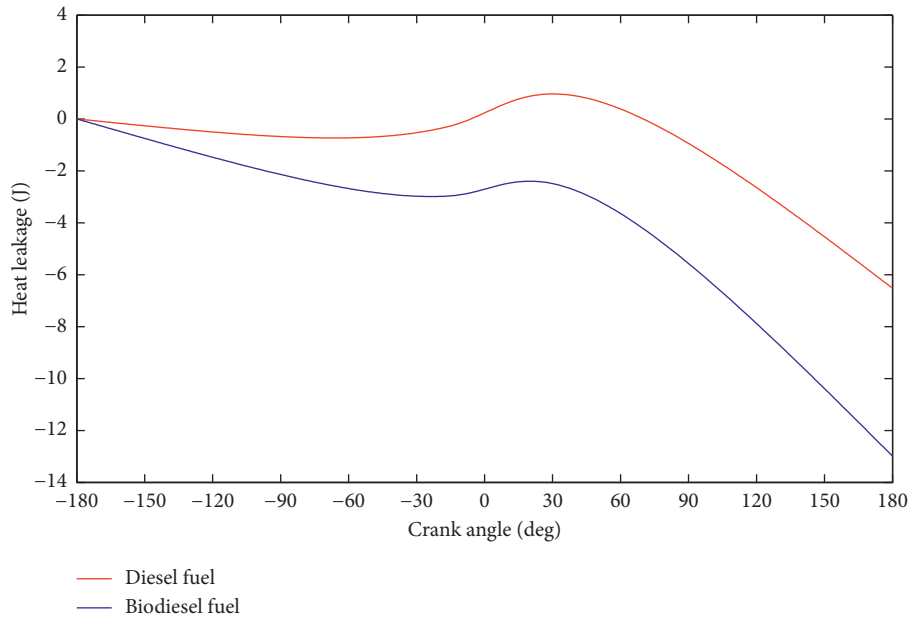

Figure 5: Heat leakage comparison of biodiesel and diesel fuels.

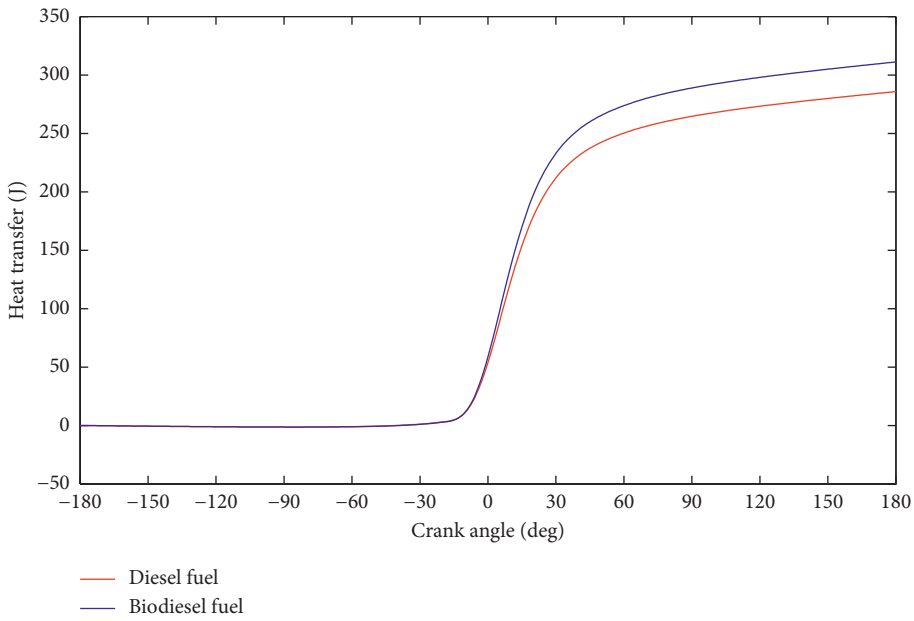

Figure 6: Heat transfer comparison of biodiesel and diesel fuels.

unburned gas is quite uniform in temperature, but the burned gas is not. Due to the progressive burning, a temperature gradient develops in the burned gas. The in-cylinder temperature evolution depends on the oxygen percentage of the fuel, which is why the biodiesel fuel with higher oxygen content than diesel fuel experiences complete combustion, leading to a higher peak and exhaust gas temperature. A higher cetane number decreases the premixing time. Contents which are not burned in the most important combustion phase continue to burn in the late combustion phase indicating the higher heat release rate curve of biodiesel fuels. This can be another reason that the biodiesel fuel has a higher exhaust gas temperature than diesel fuel. It is seen from Figure 8 that the influence of the cetane number and oxygen concentration on temperature are more dominant that the one of lower heating value and latent heat of vaporization on account of raising peak combustion temperature in the engine combustion chamber. The cylinder temperature is higher due to the higher cetane number of the biodiesel fuel than of diesel fuel. The maximum temperature for biodiesel is 2350 K, whereas for diesel fuel, the combustion temperature is 2300 K.

Figures 9–11 illustrate the adiabatic flame temperatures with respect to steam injection ratios. It is clearly observed

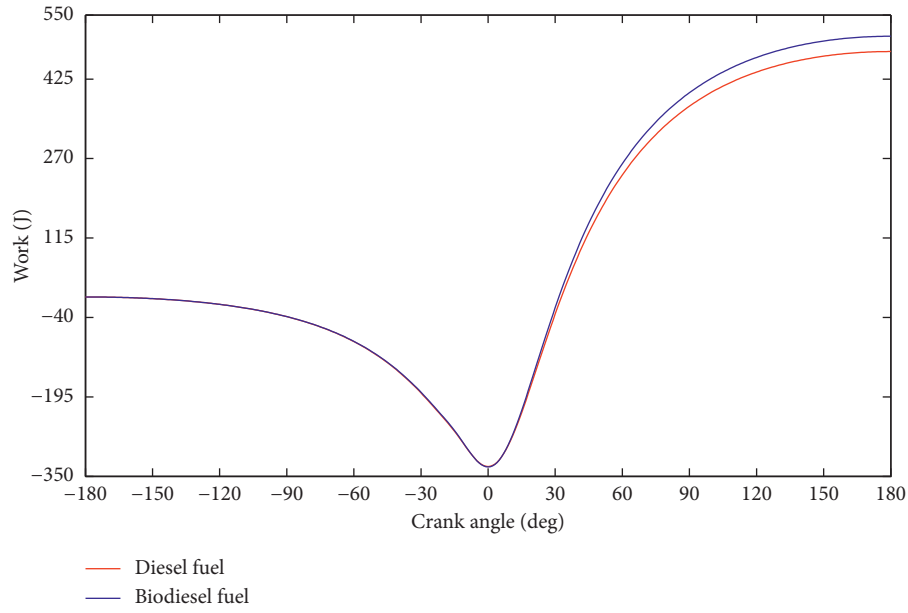

Figure 7: Work comparison of biodiesel and diesel fuels.

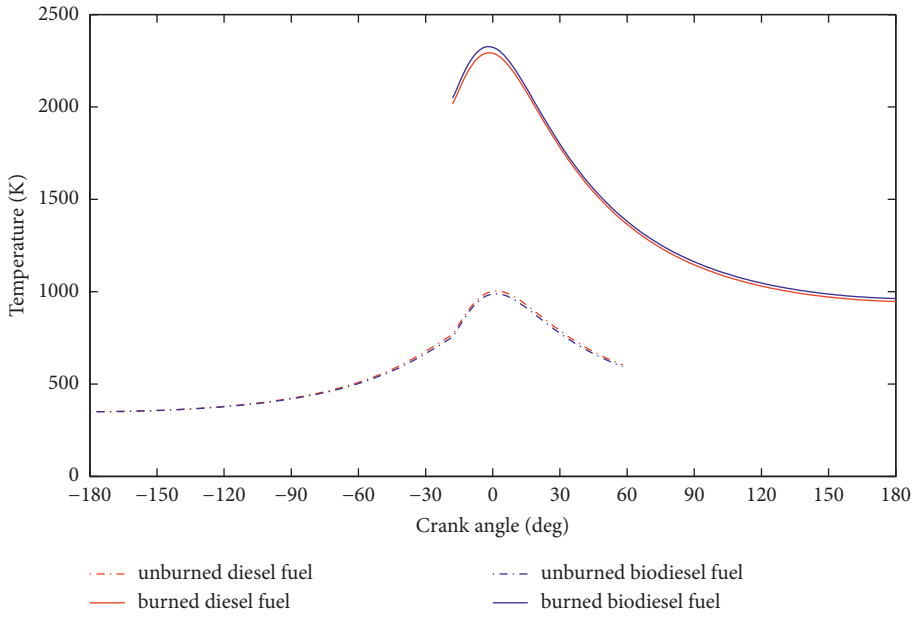

Figure 8: Temperature comparison of biodiesel and diesel fuels.

that the adiabatic flame temperatures of the diesel fuel are higher than the ones of the biodiesel fuel under these combustion conditions. The diesel fuel has the maximum flame temperatures under these combustion conditions. As may be seen from the figures, steam reduces the adiabatic flame temperatures, as the heat capacity of the steam is greater than the ones of the other combustion products.

Increased NO emission is resulted with diesel fuel because of the stoichiometric adiabatic flame temperature of diesel fuel which is higher than the one of biodiesel fuel as illustrated in Figure 10. The effect of steam injection on the combustion of biodiesel and diesel fuels is that the formation of the combustion products such as CO_2, N_2, O_2, CO, H, O, OH, and NO is decreased and the specific heat increases as steam injection increases [32]. Therefore, the steam injection method can reduce the exhaust NO emission while the engine performance increases.

Figure 12 shows the temperature-time history of the first element to burn. At the time an element burns, its nitric oxide concentration is close to zero but finite because of the residual gas present. Since the chemistry is not fast enough to assume the process is quasi-static, it is rate controlled. Once the element is burned, the equilibrium concentration is high, whereas the nonequilibrium concentration is low. Each element tries to equilibrate; if the equilibrium concentration is higher than the nonequilibrium concentration, then nitric

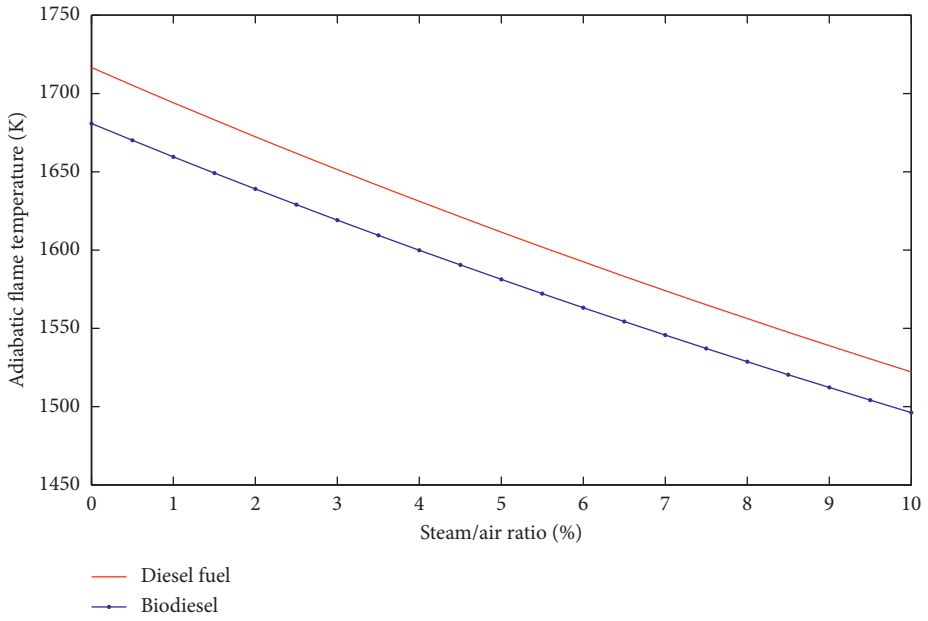

Figure 9: Adiabatic flame temperature comparison of biodiesel and diesel fuels at $\phi = 0.6$.

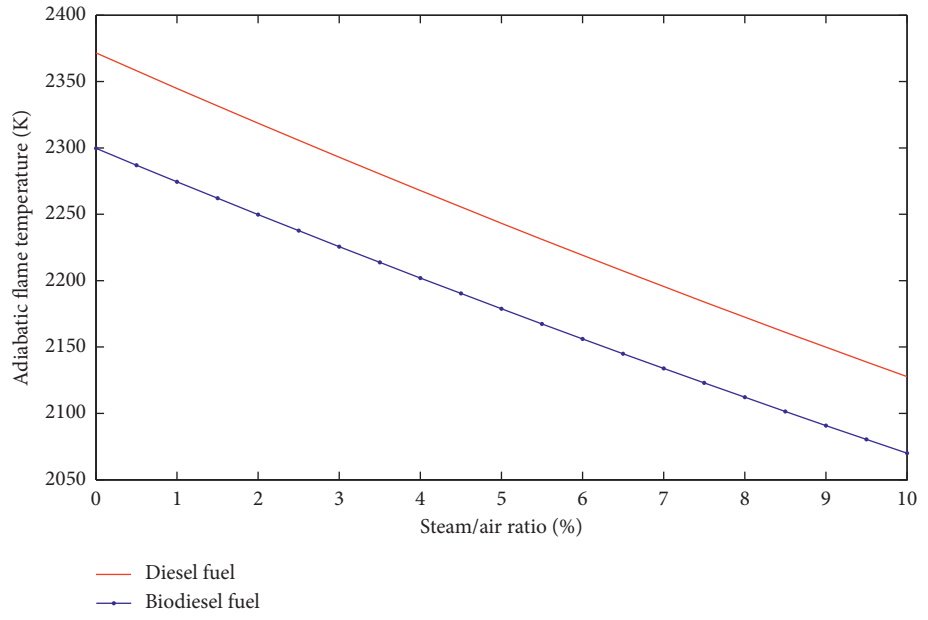

Figure 10: Adiabatic flame temperature comparison of biodiesel and diesel fuels at $\phi = 1.0$.

oxides tend to form, whereas they tend to decompose if the equilibrium concentration is less than the nonequilibrium concentration.

The chemical reaction rates increase strongly with temperature. As a result, there are large differences between the nitric oxide concentrations in the first and last elements. Furthermore, it can be seen that when the temperatures drop to about 2000 K, the decomposition rate becomes very slow and it may be said that the nitric oxides freeze at a concentration greater than the equilibrium concentration values. The total amount of nitric oxide that appears is the exhaust that is computed by summing the frozen mass fractions for all the fluid elements. The comparison of the calculated and experimental nitric oxide concentration values at the exhaust for the two fuels shows a highly satisfactory coincidence. The calculated and measured nitric oxide concentration values of biodiesel fuel are 927.7 ppm and 954.4 ppm, respectively. Also, the computed and experimental nitric oxide concentration values of diesel fuel are 1004.4 ppm and 1019.4 ppm, respectively.

It is well known that the NO formation rate strongly depends on peak temperature and duration of combustion at peak temperature in the cylinder. Thus, when the steam injection is performed, peak temperatures decreased compared to the ones without steam injection.

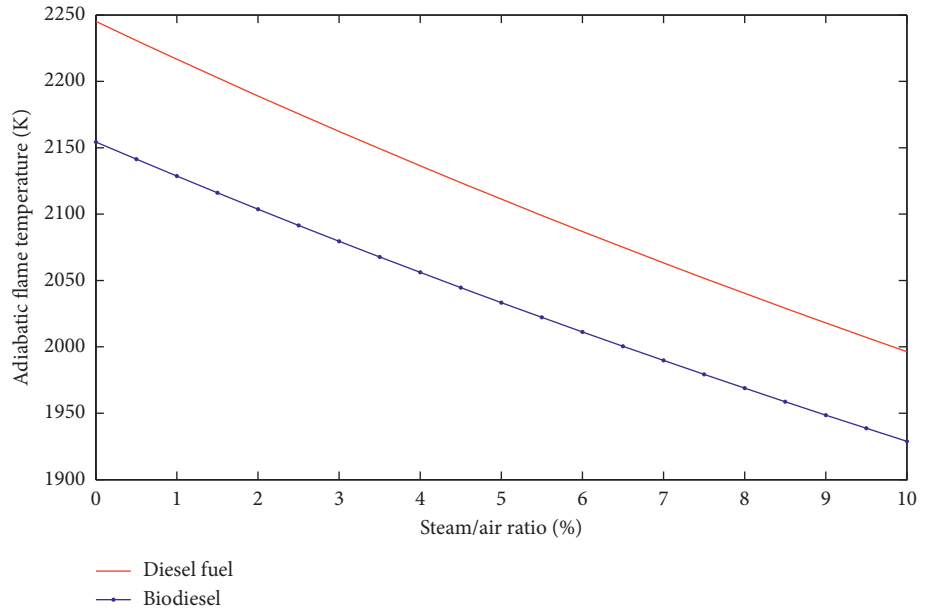

Figure 11: Adiabatic flame temperature comparison of biodiesel and diesel fuels at $\phi = 1.2$.

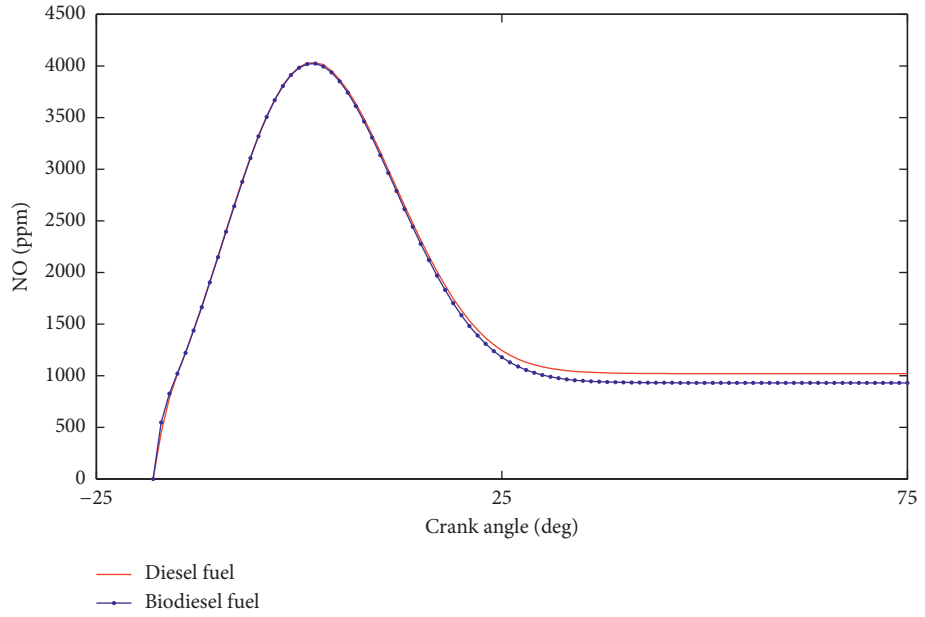

Figure 12: NO concentration comparison of biodiesel and diesel fuels.

4. Conclusion

In this study, the combustion characteristics and NO formation characteristics of a compression ignition engine fuelled with biodiesel and diesel fuels have been simulated by using a two-zone thermodynamic combustion model. The equilibrium combustion model is used to provide mole fractions of combustion products. The results of biodiesel fuel are compared with the ones of diesel fuel in this study. The results obtained from biodiesel fuel are compared with the ones of diesel fuel in terms of performance, adiabatic flame temperatures, and NO emissions. The results showed that the steam injection method could decrease NO_x emissions and improve the engine performances. The calculated and experimental nitric oxide concentration values of diesel fuel were very well matched. The highly satisfactory coincidences observed strengthened the belief that the model worked correctly.

Abbreviations

EGR: Exhaust gas recirculation
BSFC: Brake-specific fuel consumption
CN: Cetane number
c_p: Constant pressure specific heat, $kJ.kg^{-1}$
c_v: Constant volume specific heat, $kJ.kg^{-1}$

BTE: Brake thermal efficiency
FA_S: Stoichiometric fuel/air ratio by mass
h: Specific enthalpy, $kJ.kg^{-1}$
HCCI: Homogeneous charge compression ignition
LHV: Lower heating value
p: Pressure, Pa
ppm: Parts per million
RGF: Residual gas fraction
rpm: Revolutions per minute
s: Specific entropy, $kJ.kg^{-1}.K^{-1}$
T: Temperature, K
u: Specific internal energy, $kJ.kg^{-1}$
v: Specific volume, $m^3.kg^{-1}$
x: Mass fraction burned.
ϕ: Equivalence ratio
ω: Angular velocity.
a: Air
b: Burned
f: Fuel
l: Leak
st: Stoichiometric
u: Unburned.

Data Availability

No data were used in this research except the experimental pressure data for biodiesel fuel and diesel fuel provided. The authors carried out computational simulation to obtain the results of the research.

Conflicts of Interest

The authors declare that they have no conflicts of interest.

Acknowledgments

The authors would like to sincerely thank Dr. Merlin Ayissi for providing the experimental pressure data for biodiesel fuel and diesel fuel.

References

[1] S.-Y. No, "Inedible vegetable oils and their derivatives for alternative diesel fuels in CI engines: a review," *Renewable and Sustainable Energy Reviews*, vol. 15, no. 1, pp. 131–149, 2011.

[2] A. K. Agarwal, "Biofuels (alcohols and biodiesel) applications as fuels for internal combustion engines," *Progress in Energy and Combustion Science*, vol. 33, no. 3, pp. 233–271, 2007.

[3] E. Abu-Nada, I. Al-Hinti, A. Al-Sarkhi, and B. Akash, "Thermodynamic modeling of spark-ignition engine: effect of temperature dependent specific heats," *International Communications in Heat and Mass Transfer*, vol. 33, no. 10, pp. 1264–1272, 2006.

[4] E. Abu-Nada, I. Al-Hinti, B. Akash, and A. Al-Sarkhi, "Thermodynamic analysis of spark-ignition engine using a gas mixture model for the working fluid," *International Journal of Energy Research*, vol. 31, no. 11, pp. 1031–1046, 2007.

[5] E. Abu-Nada, I. Al-Hinti, A. Al-Sarkhi, and B. Akash, "Effect of piston friction on the performance of SI engine: a new thermodynamic approach," *Journal of Engineering for Gas Turbines and Power*, vol. 130, no. 2, pp. 022802–22811, 2008.

[6] E. Abu-Nada, B. Akash, I. Al-Hinti, and A. Al-Sarkhi, "Performance of a spark ignition engine under the effect of friction using a gas mixture model," *Journal of the Energy Institute*, vol. 82, no. 4, pp. 197–205, 2009.

[7] L. Chen, C. Wu, F. Sun, and S. Cao, "Heat transfer effects on the net work output and efficiency characteristics for an air-standard Otto cycle," *Energy Conversion and Management*, vol. 39, no. 7, pp. 643–648, 1998.

[8] A. Parlak, "Comparative performance analysis of irreversible dual and diesel cycles under maximum power conditions," *Energy Conversion and Management*, vol. 46, no. 3, pp. 351–359, 2005.

[9] S.-S. Hou, "Heat transfer effects on the performance of an air standard dual cycle," *Energy Conversion and Management*, vol. 45, no. 18-19, pp. 3003–3015, 2004.

[10] O. A. Ozsoysal, "Heat loss as a percentage of fuel's energy in air standard Otto and Diesel cycles," *Energy Conversion and Management*, vol. 47, no. 7-8, pp. 1051–1062, 2006.

[11] J. Zheng and J. A. Caton, "Use of a single-zone thermodynamic model with detailed chemistry to study a natural gas fueled homogeneous charge compression ignition engine," *Energy Conversion and Management*, vol. 53, no. 1, pp. 298–304, 2012.

[12] H. Xu, F. Liu, and Z. Wang, "A detailed numerical study of NOx kinetics in counterflow Methane diffusion flames: effects of fuel-side versus oxidizer-side dilution," *Journal of Combustion*, vol. 2021, Article ID 6642734, 15 pages, 2021.

[13] V. Dhana Raju, H. Venu, and L. Subramanic, "An experimental assessment of prospective oxygenated additives on the diverse characteristics of diesel engine powered with waste tamarind biodiesel," *Energy*, vol. 203, p. 117821, 2020.

[14] V. Dhana Raju, P. S. Kishore, K. Nanthagopal, and B. B.Ashok, "An experimental study on the effect of nanoparticles with novel tamarind seed methyl ester for diesel engine applications," *Energy Conversion and Management*, vol. 164, pp. 655–666, 2018.

[15] Ö. Can, İ. Çelikten, and N. Usta, "Effects of ethanol addition on performance and emissions of a turbocharged indirect injection diesel engine running at different injection pressures," *Energy Conversion and Management*, vol. 45, no. 15-16, pp. 2429–2440, 2004.

[16] C. Sayin, "Engine performance and exhaust gas emissions of methanol and ethanol–diesel blends," *Fuel*, vol. 89, p. 34105, 2010.

[17] C. Sayin and M. Canakci, "Effects of injection timing on the engine performance and exhaust emissions of a dual-fuel diesel engine," *Energy Conversion and Management*, vol. 50, no. 1, pp. 203–213, 2009.

[18] J. Huang, Y. Wang, S. Li, A. P. Roskilly, Y. Hongdong, and H. Li, "Experimental investigation on the performance and emissions of a diesel engine fuelled with ethanol–diesel blends," *Applied Thermal Engineering*, vol. 29, no. 11–12, pp. 2484–2490, 2009.

[19] C. D. Rakopoulos, K. A. Antonopoulos, and D. C. Rakopoulos, "Experimental heat release analysis and emissions of a HSDI diesel engine fueled with ethanol-diesel fuel blends," *Energy*, vol. 32, no. 10, pp. 1791–1808, 2007.

[20] E. A. Ajav, B. Singh, and T. K. Bhattacharya, "Experimental study of some performance parameters of a constant speed stationary diesel engine using ethanol-diesel blends as fuel," *Biomass and Bioenergy*, vol. 17, no. 4, pp. 357–365, 1999.

[21] D.-g. Li, H. Zhen, L. Xingcai, Z. Wu-gao, and Y. Jian-guang, "Physico-chemical properties of ethanol-diesel blend fuel and

its effect on performance and emissions of diesel engines," *Renewable Energy*, vol. 30, no. 6, pp. 967–976, 2005.

[22] A. Bilgin, O. Durgun, and Z. Sahin, "The effects of diesel-ethanol blends on diesel engine performance," *Energy Sources*, vol. 24, no. 5, pp. 431–440, 2002.

[23] M. Y. E. Selim, "Effect of exhaust gas recirculation on some combustion characteristics of dual fuel engine," *Energy Conversion and Management*, vol. 44, no. 5, pp. 707–721, 2003.

[24] G. H. Abd-Alla, H. A. Soliman, O. A. Badr, and M. F. Abd-Rabbo, "Effects of diluent admissions and intake air temperature in exhaust gas recirculation on the emissions of an indirect injection dual fuel engine," *Energy Conversion and Management*, vol. 42, no. 8, pp. 1033–1045, 2001.

[25] N. Samec, K. Breda, and R. W. Dibble, "Numerical and experimental study of water/oil emulsified fuel combustion in a diesel engine," *Fuel*, vol. 81, no. 16, pp. 2035–2044, 2002.

[26] F. Bedford, C. Rutland, P. Dittrich, A. Raab, and F. Wirbelit: Effects of Direct Water Injection on DI Diesel Engine Combustion.

[27] G. Gonca, B. Sahin, Y. Ust, A. Parlak, and A. Safa, "Comparison of steam in jected diesel engine and miller cycled diesel engine by using two-zone combustion or two zone combustion instead of two zonecombustion," *International Symposium on Combustion*, vol. 16, pp. 115–125, 2012.

[28] A. Parlak, V. Ayhan, Y. Üst et al., "New method to reduce NOx emissions of diesel engines: electronically controlled steam injection system," *Journal of the Energy Institute*, vol. 85, no. 3, pp. 135–139, 2012.

[29] İ. Cesur, A. Parlak, V. Ayhan, B. Boru, and G. Gonca, "The effects of electronic controlled steam injection on spark ignition engine," *Applied Thermal Engineering*, vol. 55, no. 1-2, pp. 61–68, 2013.

[30] G. Kökkülünk, G. Gonca, V. Ayhan, İ. Cesur, and A. Parlak, "Theoretical and experimental investigation of diesel engine with steam injection system on performance and emission parameters," *Applied Thermal Engineering*, vol. 54, no. 1, pp. 161–170, 2013.

[31] B. W. Millington and E. R. Hartles, *Frictionnal Losses in Diesel Engines*, SAE Paper, Warrendale, PA, USA, no. 680590, 1968.

[32] K. Görkem, G. Gonca, V. Ayhan, I. Cesur, and Adnan Parlak, "Theoretical and experimental investigation of diesel engine with steam injection system on performance and emission parameters," *Applied Thermal Engineering*, vol. 54, pp. 161–170, 2013.

[33] G. A. Lavoie, J. B. Heywood, and J. C. Keck, "Experimental and theoretical study of nitric oxide formation in internal combustion engines," *Combustion Science and Technology*, vol. 1, no. 4, pp. 313–326, 1970.

[34] J. P. G. Shou, M. Obounou, T. C. Kofané, and M. H. Babikir, "Investigation of the effects of steam injection on equilibrium products and thermodynamic properties of diesel and biodiesel fuels," *Journal of Combustion*, vol. 2020, Article ID 2805125, 14 pages, 2020.